Transport and optical response of molecular junctions driven by surface plasmon polaritons

Maxim Sukharev[1,*] and Michael Galperin[2,†]
[1]*Department of Applied Sciences and Mathematics, Arizona State University at the Polytechnic Campus, Mesa, Arizona 85212, USA*
[2]*Department of Chemistry & Biochemistry, University of California at San Diego, La Jolla, California 92093, USA*
(Received 12 November 2009; revised manuscript received 28 January 2010; published 7 April 2010)

We consider a biased molecular junction subjected to external time-dependent electromagnetic field. The field for two typical junction geometries (bowtie antennas and metal nanospheres) is calculated within finite-difference time-domain technique. Time-dependent transport and optical response of the junctions is calculated within nonequilibrium Green's-function approach expressed in a form convenient for description of multilevel systems. We present numerical results for a two-level (highest occupied molecular orbital-lowest unoccupied molecular orbital) model and discuss influence of localized surface plasmon-polariton modes on transport.

DOI: 10.1103/PhysRevB.81.165307 PACS number(s): 85.65.+h, 73.63.Kv, 78.67.Hc, 78.20.Bh

I. INTRODUCTION

Optical properties of structures composed of noble metals have long been attracting a considerable attention due to unique features of such systems in the visible spectrum.[1–4] Recent advances in fabrication techniques[5] along with a tremendous progress in laser technologies opened new venues for application of plasmonic materials in biology,[6] integrated optics,[7] nanoscale imagining,[8] and single-molecule manipulation.[9] Physics of surface plasmon phenomenon is relatively simple and has long been studied.[10,11] In brief, coherent oscillations of conductive electrons in a skin layer of metal known as plasmons are capable of producing strong local electromagnetic (EM) fields in the near-field region. It has been reported that such "hot" spots can be localized within 10 nm or less. This along with a great sensitivity to initial conditions and geometry makes plasmonic structures so attractable for atom/molecule manipulations.

A natural combination of nanoplasmonics and molecular response to the generated field started to appear as molecular nanopolaritonics,[12,13] which studies molecular influence on field propagation, and as a tool for developing molecular switches.[14] The latter utilizes nonadiabatic alignment of a molecule on semiconductor surface under a tip of scanning tunneling microscope.

Recent developments in experimental techniques capable of measuring optical response of current-carrying molecular junctions[15–17] lead to theoretical formulations suitable for simultaneous description of both transport and optical properties of molecular devices.[18,19]

While experimental data are measured in real time, theoretical description of both transport and optical response so far has mostly been focused on a steady-state description. Time-dependent transport usually is treated either within kinetic theory[20,21] or within time-dependent density-functional approach.[22–24] The former generally misses broadening of molecular states due to coupling to macroscopic contacts[25–27] and information on coherence,[28] although interesting generalizations started to appear.[29] Limitations of the latter are due to absence of developed pseudopotentials and fundamental necessity to treat finite (closed) systems (see, e.g., Ref. 30 for discussion). An alternative approach, based on nonequilibrium Green's-function (NEGF) technique, was initially formulated in Refs. 31–33. This approach is a natural choice for description of open nonequilibrium systems. Moreover, it provides possibility to describe response of a molecular junction initially under bias to external time-dependent perturbation (e.g., laser field).

Here we consider influence of external field specific for particular geometry on transport properties and optical response of molecular junction. While formulation of time-dependent transport within NEGF is general,[31,32] all the applications so far were restricted to resonant single-level models only. We propose a variant of the scheme capable of dealing with many-level systems. The exact calculations are compared to adiabatic pumping regime, frequent in the literature on time-dependent transport,[34,35] were at the lowest order, the problem is reduced to a set of quasisteady-state solutions with time-dependent (slow time scale) parameters. Also we generalize our previous consideration of steady-state optical response of current-carrying junctions[18,36] to a time-dependent situation.

First attempts to go beyond adiabatic approximation in NEGF appeared in the literature.[37,38] Reference 37 studies high-frequency characteristics of a nanotube transistor in the presence of time-dependent potentials at nontransport terminals. Reference 38 considers short-time transient dynamics of a junction in the off-resonant tunneling regime. Both approaches use two-dimensional time (or energy) grids in the simulations, which effectively restricts consideration to short times (or high frequencies). The latter reference also includes into consideration electron-electron interaction within perturbation theory. Here we focus on formulation of an approximate scheme capable of going beyond short-time dynamics restriction. Our interest in optical response of a molecular junction (in particular, fluorescence) naturally focuses on the resonant tunneling regime. Note that while the formulation below is within standard NEGF approach, similar consideration in the language of many-body states, i.e., employing the Hubbard NEGF approach,[39] technically will not be much different. We do not expect however qualitative difference in results for a simple model employed for demonstration purposes, thus for simplicity we employ here standard NEGF machinery. Similar to Ref. 38, we study transient behavior of a molecular junction but we focus on response of a junction initially at steady state to laser pulse.

Our goals are: (1) introduce NEGF as an approach capable of treating time-dependent properties (current and fluorescence) of molecular junction (time-dependent optical response has not been treated previously) and (2) combine transport calculations with external time-dependent radiation field calculated for realistic junction geometries. The paper is not an *ab initio* calculation. Its purpose is to demonstrate the approach within a simple (but straightforwardly extensible) model. However, even within the model-type calculations with realistic parameters, one can judge about importance of influence of the field on transport and optical response of a junction.

The paper is organized as follows. Section II describes methodology of EM field calculation for different junction geometries. Section III presents a transport model of molecular junction. Electric field calculated in Sec. II is used as an external driving force in transport simulations. Methodology of these simulations is presented in Sec. IV. Adiabatic pumping version is discussed in Sec. V. Numerical results are presented in Sec. VI. Section VII concludes.

II. ELECTROMAGNETIC FIELD SIMULATIONS

Among various numerical techniques that allow one to predict optical properties of plasmonic systems, the finite-difference time-domain approach (FDTD) is considered to be the most efficient and yet relatively simple. FDTD yields data in perfect agreement with experimental measurements and results obtained within other techniques.[40] We simulate optical response of metal structures utilizing FDTD approach in which Maxwell equations are discretized in space and time following Yee's algorithm.[41] Dispersion of dielectric constant of metal, $\varepsilon(\omega)$, is taken in the form of the Drude model,

$$\varepsilon(\omega) = \varepsilon_r - \frac{\omega_p^2}{\omega^2 - i\Gamma\omega} \tag{1}$$

with numerical parameters describing silver for the wavelengths of interest $\varepsilon_r = 8.26$, $\omega_p = 1.76 \times 10^{16}$ rad/s, and $\Gamma = 3.08 \times 10^{14}$ rad/s.

Material dispersion condition, Eq. (1), leads to equation describing time evolution of current density, $\vec{J}$, in metal,[42]

$$\frac{\partial \vec{J}}{\partial t} = -\Gamma \vec{J} + \varepsilon_0 \omega_p^2 \vec{E}, \tag{2}$$

where $\vec{E}$ is the electric field amplitude and ε_0 is the dielectric permittivity of vacuum. Equation (2) along with the Maxwell equations form a set of equations which are solved with the auxiliary differential equation method.[43]

For simulations of open systems, one needs to impose artificial absorbing boundaries in order to avoid reflection of outgoing EM waves back to the simulation domain. Among various approaches that address this numerical issue, the perfectly matched layers (PMLs) technique[44] is considered to be the most adequate. It reduces the reflection coefficient of outgoing waves at the simulation region boundary to 10^{-8}. Essentially, the PML approach surrounds the simulation domain by thin layers of nonphysical material that efficiently absorbs outgoing waves incident at any angle. We implement the most efficient and least memory intensive method, convolution perfectly matched layers (CPMLs)[45] absorbing boundaries, at all six sides of the three-dimensional modeling cube. Through extensive numerical experimentation, we have empirically determined optimal parameters for the CPML boundaries that lead to almost no reflection of the outgoing EM waves at all incident angles. Spatial steps, $\delta x = \delta y = \delta z$, along all axes are fixed at 1 nm to assure numerical convergence and the temporal step is $\delta t = \delta x/(2c)$, where c is the speed of light in vacuum.

Numerical integration of Maxwell equations on a grid within the FDTD framework was performed at the local ASU home-built supercomputer utilizing 120 processors. An average execution time for our codes is around 20 min.

A particular advantage of the FDTD method is its ability to obtain the optical response of the structure (assuming linear response) in the desired spectral range in a single run.[46] The system is excited with an ultrashort optical pulse constructed from Fourier components spanning the frequency range of interest. Next, Maxwell's equations are propagated in time for several hundred femtoseconds and the components of the EM field are detected at the point of interest (for our purposes, we consider the detection point where a molecule is located). Fourier transforming the detected EM field on the fly yields intensities that can be easily processed into the spectral response. Note, FDTD allows the direct evaluation of the intensity enhancement relative to the incident field. This provides capability for straightforward evaluation of "coupling efficiency" in plasmonic structures within spectral range of interest.

Since FDTD is a time-domain integrator, it is straightforward to simulate electric field at any spatial point at any time. Below we use electric field in a "hot spot" as a time-dependent driving force in simulations of quantum transport and optical response of a molecular junction. Note that electric field calculated within FDTD contains both correct peak amplitudes and time dependence. The latter is important in the case of resonant excitation of plasmonic systems with a short laser pulse, when metal-induced time-dependent phase is significantly pronounced.[47,48] This phase results in noticeable changes in response of a molecular junction (see discussion at the end of Sec. VI).

III. MODEL

We consider a two-level system $\varepsilon_{1,2}$, representing highest occupied (HOMO) and lowest unoccupied (LUMO) molecular orbitals (or ground and excited states in the many-body language), coupled to two macroscopic electrodes L and R. The electrodes are considered to be each in its own equilibrium with electrochemical potentials μ_L and μ_R, respectively. We assume that the driving (laser field) frequency is smaller than the plasma frequency so that usual division of the junction into nonequilibrium molecule coupled to free-electron reservoirs (metallic contacts) is relevant (for a thorough discussion of the assumptions see Ref. 31). Local field at the position of the molecule is assumed to be an external time-dependent driving force causing excitation in the mol-

ecule. Following Ref. 18 in addition to charge transfer between contacts and molecule, we introduce also energy transfer (coupling of molecular excitations to electron-hole excitations in the contacts). Molecular excitations are coupled to a bath of free photon modes (accepting modes), which serve as a measurement device of molecular optical response. Hamiltonian of the system is

$$\hat{H} = \hat{H}_0 + \hat{V}, \tag{3}$$

$$\hat{H}_0 = \sum_{i=1,2} \varepsilon_i \hat{d}_i^\dagger \hat{d}_i - (\vec{\mu}_{12}\hat{d}_1^\dagger \hat{d}_2 + \vec{\mu}_{21}\hat{d}_2^\dagger \hat{d}_1)\vec{E}(t) + \sum_{k\in\{L,R\}} \varepsilon_k \hat{c}_k^\dagger \hat{c}_k + \sum_\alpha \omega_\alpha \hat{a}_\alpha^\dagger \hat{a}_\alpha + \sum_{i=1,2;k\in\{L,R\}} (V_{ki}^{et}\hat{c}_k^\dagger \hat{d}_i + V_{ik}^{et}\hat{d}_i^\dagger \hat{c}_k), \tag{4}$$

$$\hat{V} = \sum_{k\neq k'\in\{L,R\}} (V_{kk'}^{eh}\hat{c}_k^\dagger \hat{c}_{k'}\hat{d}_2^\dagger \hat{d}_1 + V_{k'k}^{eh}\hat{c}_{k'}^\dagger \hat{c}_k \hat{d}_1^\dagger \hat{d}_2) + \sum_\alpha (V_\alpha^p \hat{a}_\alpha \hat{d}_2^\dagger \hat{d}_1 + V_\alpha^{p*}\hat{a}_\alpha^\dagger \hat{d}_1^\dagger \hat{d}_2). \tag{5}$$

Here $\hat{d}_i^\dagger$ ($\hat{d}_i$) and $\hat{c}_k^\dagger$ ($\hat{c}_k$) are creation (annihilation) operators for an electron in the state i of the molecule and state k of the contact, respectively. $\hat{a}_\alpha^\dagger$ ($\hat{a}_\alpha$) is creation (annihilation) operator for a photon in the state α, $\vec{E}(t)$ is external time-dependent field, and $\vec{\mu}_{ij}=\langle i|\hat{\vec{\mu}}|j\rangle$ is matrix element of the molecular (vector) dipole operator between states i and j of the molecule $(i,j=1,2)$. We assume $\vec{\mu}_{11}=\vec{\mu}_{12}=0$ (or alternatively one can think about these contributions being included into definition of the state energies $\varepsilon_{1,2}$). V^{et} and V^{eh} are matrix elements for electron and energy transfer between molecule and contacts, and V^p represents optical response of the molecule. Note, the form of energy-transfer operator is a standard model in exciton theory.[49]

Classical field $E(t)$ and quantum operators $\hat{a}$ ($\hat{a}^\dagger$) represent different modes of radiation field. It is customary to consider a "pumping mode" separately from the rest of the field modes (accepting modes).[18] The idea behind such separation is neglect of molecular backaction on the driving force (the pumping mode). The "accepting modes" serve as an optical detector for photon flux coming out of the system. Since in the current consideration external field is calculated as a classical driving force, it is convenient to introduce it in the Hamiltonian in the usual semiclassical fashion. Such mixed quantum-classical representation is used in conventional optical spectroscopy.[50] Also this way we can treat external field of arbitrary time dependence exactly (i.e., beyond perturbation theory).

Below we consider two approaches to transport and optical response simulations within the model: exact solution of the time-dependent Dyson equation and adiabatic pumping regime. The former is similar to the procedure described in Refs. 31–33, however it is presented in a form convenient for treating a multilevel molecular system (see Sec. IV for discussion). The latter assumes that $\vec{E}(t)$ can be represented as a product of an oscillation of frequency ω_0 with a slowly varying in time (on the time scale of ω_0) envelope $\vec{F}(t)$. In the spirit of the Born-Oppenheimer approximation, $\vec{F}(t)$ is considered as a parameter when solving electronic part of the problem. In this case, the form of molecule-field interaction becomes (within rotating wave approximation)

$$-(\vec{\mu}_{12}\hat{d}_1^\dagger \hat{d}_2 e^{i\omega_0 t} + \vec{\mu}_{21}\hat{d}_2^\dagger \hat{d}_1 e^{-i\omega_0 t})\vec{F}(t). \tag{6}$$

Details of the approach are presented in Sec. V.

As usual, we treat the perturbation $\hat{V}$, Eq. (5), at the second order and within noncrossing approximation.[49] Self-energy due to energy transfer (on the Keldysh contour) is[18]

$$\Sigma^{eh}(\tau_1,\tau_2) = \sum_{k\neq k'\in\{L,R\}} |V_{kk'}^{eh}|^2 g_k(\tau_2,\tau_1) g_{k'}(\tau_1,\tau_2) \times \begin{bmatrix} G_{22}(\tau_1,\tau_2) & G_{21}(\tau_1,\tau_2) \\ G_{12}(\tau_1,\tau_2) & G_{11}(\tau_1,\tau_2) \end{bmatrix}, \tag{7}$$

where G_{ij} are molecular Green's functions in the lowest order of expansion associated with the Hamiltonian $\hat{H}_0$, Eq. (4), and g_k are Green's functions of free electrons in the contacts. Self-energy due to coupling to photon bath is[18]

$$\Sigma^p(\tau_1,\tau_2) = \sum_\alpha |V_\alpha^p|^2 \begin{bmatrix} iF_\alpha(\tau_2,\tau_1)G_{22}(\tau_1,\tau_2) & \delta(\tau_1,\tau_2)\int_{-\infty}^{t_1} dt' \rho_{12}(t')F_\alpha^a(t'-t_1) \\ \delta(\tau_1,\tau_2)\int_{-\infty}^{t_2} dt' F_\alpha^r(t_1-t')\rho_{21}(t') & iF_\alpha(\tau_1,\tau_2)G_{11}(\tau_1,\tau_2) \end{bmatrix}, \tag{8}$$

where F_α is Green's function for free photon and $\rho_{ij}(t)\equiv -iG_{ij}^<(t,t)$ is nonequilibrium reduced density matrix. We use coupling to accepting modes, second term in Eq. (5) only to derive expression for fluorescence of the junction, Eq. (19), and disregard it when calculating system Green's functions. This assumption is justified by smallness of the reasonable coupling parameter (see Ref. 18 for details).

Below we present approaches to calculate time-dependent current and optical response of driven molecular junction.

IV. TIME-DEPENDENT TRANSPORT

We are interested in calculating time-dependent current and optical response of the junction. Expression for the current at the interface K ($K=L,R$) between molecule and contact is[51]

$$I_K(t) = \frac{e}{\hbar}\int_{-\infty}^{t} dt_1\ \mathrm{Tr}[\boldsymbol{\Sigma}_K^<(t,t_1)\mathbf{G}^>(t_1,t) + \mathbf{G}^>(t,t_1)\boldsymbol{\Sigma}_K^<(t_1,t) - \boldsymbol{\Sigma}_K^>(t,t_1)\mathbf{G}^<(t_1,t) - \mathbf{G}^<(t,t_1)\boldsymbol{\Sigma}_K(t_1,t)], \tag{9}$$

where Σ_K is self-energy due to coupling to contact K,

$$[\boldsymbol{\Sigma}_K^{et}(\tau_1,\tau_2)]_{ij} = \sum_{k\in K} V_{ik}^{et} g_k(\tau_1,\tau_2) V_{kj}^{et} \tag{10}$$

and r, a, $<$, and $>$ are retarded, advanced, lesser, and greater projections, respectively. In the wideband limit, when escape rate matrix

$$[\boldsymbol{\Gamma}_K(E)]_{ij} = 2\pi\sum_{k\in K} V_{ik}^{et} V_{kj}^{et} et\,\delta(E-\varepsilon_k) \tag{11}$$

is assumed to be energy independent and real part of the self-energy [Eq. (10)] is disregarded, and when time modulation is restricted to molecular subspace only, expression (9) reduces to[31]

$$I_K(t) = I_K^{in}(t) - I_K^{out}(t), \tag{12}$$

$$I_K^{in}(t) = -\frac{e}{\pi\hbar}\int_{-\infty}^{+\infty} dE f_K(E)\mathrm{Im}\ \mathrm{Tr}[\boldsymbol{\Gamma}_K\mathbf{A}^{\mathbf{r}}(t,E)], \tag{13}$$

$$I_K^{out}(t) = +\frac{e}{\hbar}\mathrm{Re}\ \mathrm{Tr}[\boldsymbol{\Gamma}_K\rho(t)], \tag{14}$$

where $f_K(E)$ is Fermi-Dirac distribution in contact K and $\mathbf{A}^r(t,E)$ is time-dependent (one-sided) Fourier transform of the retarded Green's function $\mathbf{G}^r(t,t')$,

$$\mathbf{A}^r(t,E) = \int_{-\infty}^{t} dt'\, e^{iE(t-t')}\mathbf{G}^r(t,t'). \tag{15}$$

In the absence of time-dependent driving, $\mathbf{A}^r(t,E)$ reduces to usual Fourier transform for retarded Green's function $\mathbf{G}_0^r(E)=[E-\mathbf{H}_0-\boldsymbol{\Sigma}^r(E)]^{-1}$. In general, $\boldsymbol{\Sigma}^r$ has contributions (additive within noncrossing approximation) from all the processes involved. $\rho(t)$ in Eq. (14) is reduced density matrix,

$$\rho(t) = -i\mathbf{G}^<(t,t). \tag{16}$$

Lesser and greater Green's functions are calculated from the time-dependent Dyson equation,

$$\mathbf{G}^{>,<}(t,t') = \int_{-\infty}^{t} dt_1 \int_{-\infty}^{t'} dt_2 e^{-iE(t_1-t_2)} \times \mathbf{A}^r(t_1,E)\boldsymbol{\Sigma}^{>,<}(E)\mathbf{A}^a(t_2,E), \tag{17}$$

where

$$A_{ij}^a(t,E) = \overset{*}{A}_{ji}^r(t,E) \tag{18}$$

and $\mathbf{A}^r(t,E)$ is defined in Eq. (15).

Contrary to our previous consideration,[18,36] optical response of molecular junction is calculated as a true photon flux into modes $\{\alpha\}$, rather than corresponding electronic current between molecular orbitals. We start from general expression for time-dependent photon flux into mode α (the derivation follows the corresponding procedure for electronic current, the latter can be found in, e.g., Ref. 51),

$$\begin{aligned} J_\alpha(t) &\equiv \frac{d}{dt}\langle \hat{a}_\alpha^\dagger(t)\hat{a}_\alpha(t)\rangle \\ &= |V_\alpha^p|^2\int_{-\infty}^{t} dt_1[F_\alpha^<(t,t_1)\mathcal{G}^>(t_1,t) \\ &\quad + \mathcal{G}^>(t,t_1)F_\alpha^<(t_1,t) - F_\alpha^>(t,t_1)\mathcal{G}^<(t_1,t) \\ &\quad - \mathcal{G}^<(t,t_1)F_\alpha^>(t_1,t)]. \end{aligned} \tag{19}$$

Here $\mathcal{G}$ is two-particle Green's function,

$$\mathcal{G}(\tau,\tau') \equiv -\frac{i}{\hbar}\langle T_c\hat{D}(\tau)\hat{D}^\dagger(\tau')\rangle, \tag{20}$$

where $\hat{D}\equiv\hat{d}_1^\dagger\hat{d}_2$ is molecular deexcitation operator. For empty accepting mode α, expression (19) reduces to

$$J_\alpha(t) = -2\frac{|V_\alpha^p|^2}{\hbar}\mathrm{Im}\int_{-\infty}^{t} dt_1 e^{i\omega_\alpha(t_1-t)}\mathcal{G}^<(t_1,t). \tag{21}$$

As in Ref. 18, we approximate the two-particle Green's function by zero-order (in interaction) expression,

$$\mathcal{G}^<(t_1,t) \approx -i\hbar[G_{11}^>(t,t_1)G_{22}^<(t_1,t) - \rho_{12}(t)\rho_{21}(t_1)]. \tag{22}$$

Note that if envelope change in time is slow (on the time scale of ω_α), second term on the right of Eq. (22) can be safely disregarded. In this case, expression (21) becomes equivalent to approximate expression used in Ref. 18.

Below we calculate frequency resolved,

$$\begin{aligned} J(\omega,t) &\equiv \sum_\alpha J_\alpha(t)\delta(\omega-\omega_\alpha) \\ &\approx \frac{1}{\pi\hbar}\gamma_\alpha(\omega)\mathrm{Re}\int_{-\infty}^{t} dt_1 e^{i\omega(t_1-t)}G_{11}^>(t,t_1)G_{22}^<(t_1,t) \end{aligned} \tag{23}$$

and total

$$J_{tot}(t) \equiv \int_0^\infty d\omega J(\omega,t) \tag{24}$$

photon fluxes. Here $\gamma_\alpha(\omega)\equiv 2\pi\Sigma_\alpha\delta(\omega-\omega_\alpha)$, and in simulations we use[52]

$$\gamma_\alpha(\omega) = \eta\omega e^{-\omega/\omega_c}. \tag{25}$$

To calculate time-dependent charge, Eq. (12), and photon, Eq. (21), fluxes, one needs time-dependent Fourier transform of retarded Green's function, Eq. (15). The Dyson equation for retarded Green's function is

$$\left[i\frac{\partial}{\partial t}-\mathbf{H}(t)\right]\mathbf{G}^r(t,t')-\int_{-\infty}^{+\infty}dt_1\boldsymbol{\Sigma}^r(t-t_1)\mathbf{G}^r(t_1,t')=\delta(t-t'). \tag{26}$$

Its one-sided Fourier transform leads to equation for $\mathbf{A}^r(t,E)$ in the form

$$\left(i\frac{\partial}{\partial t}-[\mathbf{H}_0(t)-E]\right)\mathbf{A}^r(t,E)-\int_{-\infty}^{+\infty}dt_1\boldsymbol{\Sigma}^r(t-t_1)\mathbf{A}^r(t_1,E)=\mathbf{I}. \tag{27}$$

We consider situation when time-dependent external field is applied at time t_0 to a biased molecular junction initially at steady state. In this case, Eq. (27) can be solved numerically starting from known initial condition $\mathbf{A}^r(t_0,E)=\mathbf{G}_0^r(E)=[E-\mathbf{H}_0^c-\boldsymbol{\Sigma}^r(E)]^{-1}$.

Alternatively, splitting $\mathbf{H}_0(t)$ into time-independent $\mathbf{H}_0^c$ and time-dependent $\mathbf{H}_0^t(t)$ parts (average over time of the time-dependent part can be included into the time-independent Hamiltonian), one can rewrite Dyson Eq. (26) in the integral form

$$\mathbf{G}^r(t,t')=\mathbf{G}_0^r(t-t')+\int_{-\infty}^{t}dt_1\mathbf{G}_0^r(t-t_1)\mathbf{H}_0^t(t_1)\mathbf{G}^r(t_1,t'). \tag{28}$$

One-sided Fourier transform of Eq. (28) leads to integral equation for $\mathbf{A}^r(t,E)$,

$$\mathbf{A}^r(t,E)=\mathbf{G}_0^r(E)+\int_{t_0}^{t}dt_1\mathbf{G}_0^r(t-t_1)e^{iE(t-t_1)}\mathbf{H}_0^c(t_1)\mathbf{A}^r(t_1,E), \tag{29}$$

where lower limit of the integral in the right is set to t_0 since $\mathbf{H}_0^t(t<t_0)=0$. Its solution is

$$\mathbf{A}^r(t,E)=\mathbf{U}_{eff}(t,t_0;E)\mathbf{G}_0^r(E), \tag{30}$$

$$\mathbf{U}_{eff}(t,t_0;E)\equiv T\exp\left[\int_{t_0}^{t}dt_1\mathbf{G}_0^r(t-t_1)e^{iE(t-t_1)}\mathbf{H}_0^t(t_1)\right]. \tag{31}$$

Effective evolution operator $\mathbf{U}_{eff}$ can be obtained by variety of methods available in the literature (see, e.g., Ref. 53, and references therein). One of the simplest schemes is cumulant (or Magnus) expansion.[50,54,55]

Note that although our consideration is restricted to the case when time-dependent driving takes place in the molecular subspace only, generalization to driving in the contacts or at the molecule-contact interface is straightforward.

V. ADIABATIC PUMPING REGIME

When time evolution of an envelope $\vec{F}(t)$, Eq. (6), is slow on the time scale of the field frequency ω_0, consideration of the time-dependent transport is simplified by invoking adiabatic assumption [treating $\vec{F}(t)$ as a parameter].

We start with Hamiltonian (3) in which interaction with driving field is written in the form presented in Eq. (6). Transforming the Hamiltonian into rotating frame of the field,[56,57]

$$\hat{\bar{H}}=e^{\hat{S}}\hat{H}e^{-\hat{S}}+\left(i\frac{\partial}{\partial t}e^{\hat{S}}\right)e^{-\hat{S}}, \tag{32}$$

$$\hat{S}=-\frac{i\omega_0 t}{2}(\hat{n}_1-\hat{n}_2), \tag{33}$$

where $\hat{n}_i=\hat{d}_i^\dagger\hat{d}_i$ $(i=1,2)$, leads to

$$\hat{\bar{H}}=\hat{\bar{H}}_0+\hat{\bar{V}}, \tag{34}$$

$$\hat{\bar{H}}_0=\sum_{i=1,2}\bar{\varepsilon}_i\hat{d}_i^\dagger\hat{d}_i-(\vec{\mu}_{12}\hat{d}_1^\dagger\hat{d}_2+\vec{\mu}_{21}\hat{d}_2^\dagger\hat{d}_1)\vec{F}(t)+\sum_{k\in\{L,R\}}\varepsilon_k\hat{c}_k^\dagger\hat{c}_k+\sum_{\alpha}\omega_\alpha\hat{a}_\alpha^\dagger\hat{a}_\alpha+\sum_{i=1,2;k\in\{L,R\}}(V_{ki}^{et}\hat{c}_k^\dagger\hat{d}_i e^{-i(-1)^i\omega_0 t/2}+\text{H.c.}), \tag{35}$$

$$\hat{\bar{V}}=\sum_{k\neq k'\in\{L,R\}}(V_{kk'}^{eh}\hat{c}_k^\dagger\hat{c}_{k'}\hat{d}_2^\dagger\hat{d}_1 e^{i\omega_0 t}+\text{H.c.})+\sum_{\alpha}(V_\alpha^p\hat{a}_\alpha\hat{d}_2^\dagger\hat{d}_1 e^{i\omega_0 t}+\text{H.c.}), \tag{36}$$

where

$$\bar{\varepsilon}_i=\varepsilon_i-(-1)^i\omega_0/2. \tag{37}$$

Within rotating wave approximation, only diagonal elements of the self-energy due to coupling to the contacts (electron transfer) Σ^{et}, Eq. (10), and self-energy due to coupling to electron-hole excitations (energy transfer) Σ^{en}, Eq. (7), survive

$$\bar{\Sigma}_{ii}^{et}(\tau_1,\tau_2)=\Sigma_{ii}^{et}(\tau_1,\tau_2)e^{i(-1)^i\omega_0(t_1-t_2)/2}, \tag{38}$$

$$\bar{\Sigma}_{ii}^{eh}(\tau_1,\tau_2)=\Sigma_{ii}^{eh}(\tau_1,\tau_2)e^{i(-1)^i\omega_0(t_1-t_2)}. \tag{39}$$

Energy transfer becomes important (and even may be dominating) at large molecule-contact separations.[58] It is of particular importance when considering optical response of excited molecule since it provides a way of radiationless relaxation.

Resulting Green's functions $\bar{G}(t_1,t_2)$ depend parametrically on slow time variable $t=(t_1+t_2)/2$ through time dependence of the envelope $\vec{F}(t)$, Eq. (35). Transforming to Wigner coordinates, taking Fourier transform in the relative coordinate t_1-t_2, and using gradient expansion,[51] leads to the following expressions for charge:

$$\bar{I}_K(t)=\sum_{n=0}^{\infty}\frac{i^n}{2^n n!}\int_{-\infty}^{+\infty}\frac{dE}{2\pi}\text{Tr}\left[\frac{\partial^n\bar{\boldsymbol{\Sigma}}^<_K(E)}{\partial E^n}\frac{\partial^n\bar{\mathbf{G}}^>(t,E)}{\partial t^n}-\frac{\partial^n\bar{\boldsymbol{\Sigma}}^>_K(E)}{\partial E^n}\frac{\partial^n\bar{\mathbf{G}}^<(t,E)}{\partial t^n}\right] \tag{40}$$

and photon

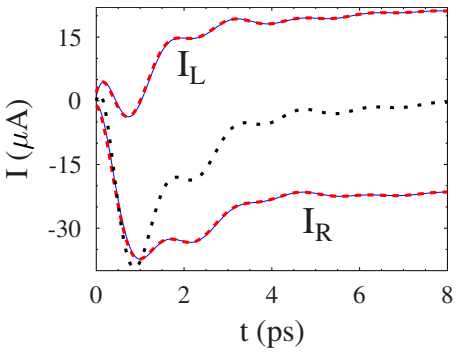

FIG. 1. (Color online) Current on the left, I_L, and right, I_R, interfaces vs time for single-level model. Numerical results (dashed line, red) are compared to analytical expression (solid line, blue). Also shown is sum of the currents, I_L+I_R at the two interfaces (dotted line, black). See text for parameters.

$$\bar{J}_a(t) = |V_\alpha^p|^2 \sum_{n,m=0}^{\infty} \frac{i^{n+m}}{2^{n+m} n!m!} \int_{-\infty}^{+\infty} \frac{dE}{2\pi} \left(\frac{\partial^n}{\partial t^n} \frac{\partial^n}{\partial E^n} \bar{G}_{11}^{>}(t,E) \right) \times \left(\frac{\partial^m}{\partial t^m} \frac{\partial^m}{\partial E^m} \bar{G}_{22}^{<}(t,E+\omega_\alpha) \right) \quad (41)$$

fluxes. Equations (40) and (41) are main results of this section. They are to be compared with general expressions (9) and (21), respectively.

VI. NUMERICAL RESULTS

We calculate time-dependent transport and optical response by invoking Runge-Kutta scheme with adaptive step size control[59] to solve numerically system of differential Eq. (27).

To check accuracy of our numerical approach, we start from a test calculation for a single-level model. Analytical solution is available for the latter.[31] In a biased junction ($\mu_L=1$ eV and $\mu_R=-1$ eV), the level is set below both chemical potentials ($\varepsilon_0=-2$ eV) so that initially the level is occupied and current through the junction is negligible (escape rates are $\Gamma_L=\Gamma_R=0.2$). At time t_0, position of the level is shifted to 0 eV (steplike modulation). Here and below, we assume Fermi distributions in the leads corresponding to room temperature $T=300$ K. Figure 1 presents transient current at the two interfaces (direction from contact into the system is taken to be positive for both currents) calculated numerically (dashed line) and with analytical solution (solid line). Also shown is sum of the currents at the two interfaces (dotted line). Outflux of electrons from initially fully populated level into the right contact leads to ringing effect. Eventually the current achieves steady state. Our numerical procedure is seen to give good correspondence with the analytical result. Below we use similar parameters for calculation of time-dependent response of the two-level system.

Calculation parameters for the model are chosen to represent realistic molecular junction. Wavelengths of external field as well as length of the pulse considered correspond to those used in experimental setups.[16] Distance between the levels of $\varepsilon_2-\varepsilon_1 \sim 2$ eV represents properly HOMO-LUMO gap in molecules.[60] The Fermi energy E_F is taken at the midpoint in the gap, which is the usual practice even in *ab initio* calculations when character of the transport (electron vs hole mediated) for particular molecule is not known. Voltage is divided symmetrically between the two sides (L and R), which corresponds to symmetric coupling of the molecule to electrodes. Escape rates $\Gamma_{11,22}$ is chosen to be 0.1 eV in accordance with experimental data on lifetime for the decay of an excess electron on molecule near metal surface.[61] We neglect cross correlation due to coupling to the contacts $\Gamma_{12,21}=0$ since interlevel distance is much bigger than the coupling strength. With characteristic molecular dipoles ~ 10 D (Ref. 62) and incident laser fields $\sim 10^8$ V/m,[63] reasonable coupling to the driving force is $10^{-3}-10^{-2}$ eV. Energy-transfer coupling has dipolar distance dependence, and reasonable choice for this parameter 0.01–0.1 eV was discussed in Refs. 18 and 58.

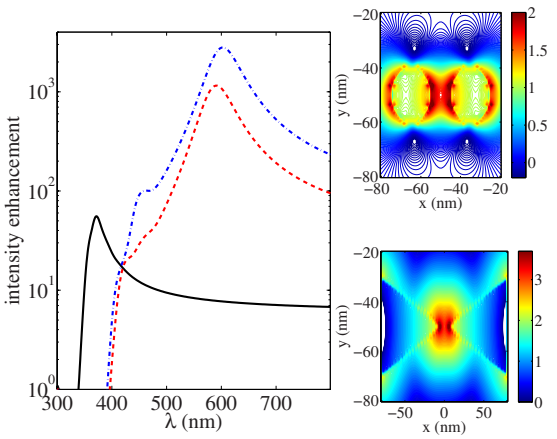

FIG. 2. (Color online) Results of FDTD simulations. Left panel shows intensity enhancement as a function of the incident wavelength (in nanometer) in logarithmic scale for two spheres of 20 nm in diameter with a gap of 10 nm (solid line, black) and bowtie antenna with a gap of 10 nm (dashed line, red), and 5 nm (dashed-dotted line, blue). Top right inset represents steady-state intensity enhancement distribution in logarithmic scale for two spheres system at the resonant wavelength of 368.202 nm. Lower right inset shows intensity distribution for the bowtie antennas with a gap of 5 nm at 602.647 nm.

We consider two geometries of a junction: a bowtie antenna electrodes and electrodes in the form of metallic spheres. Large single-molecule fluorescence measurements were reported recently for the former.[64] The latter (molecule between two metallic nanoparticles) is customary in experimental setups.

Both structures are excited by a plane wave polarized along the axis of symmetry (i.e., along the axis connecting centers of two spheres, for instance). The electric field amplitude is then detected as a function of time. Recorded amplitudes are Fourier transformed and normalized with respect to the incident-field amplitude leading to enhancement in the frequency domain.

Results of our simulations for both geometries are presented in Fig. 2 showing intensity enhancements in the main panel. As expected, bowtie structures result in noticeably higher enhancements reaching 630 centered at $\lambda=600$ nm

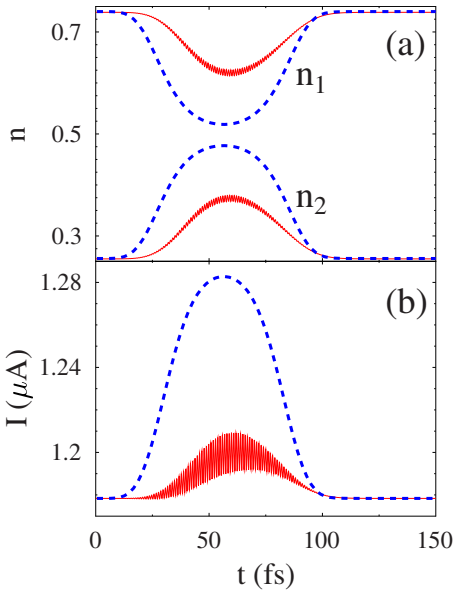

FIG. 3. (Color online) Comparison of exact numerical solution (solid line, red) to adiabatic approximation (dashed line, blue) for the two-level (HOMO-LUMO) model. Shown are (a) levels populations and (b) current at the left interface vs time. See text for parameters.

for a bowtie antenna with a gap of 5 nm. Two spheres also show significant enhancement of 55 around $\lambda=370$ nm. We note that the bowtie antenna in comparison to two spheres system exhibits two resonances. The "blue" resonance located at low wavelength corresponds to the rod lightning effect with a high enhancement localized primarily at the edges of each triangle. This feature disappears from the spectrum once sharp corners are replaced with smooth edges.[46] Top and bottom insets show intensity enhancement distributions at resonant conditions for the two spheres and bowtie antennas, respectively. We place molecule in the hot-spot regions.

Figure 3(a) shows time-dependent populations of molecular junction driven by external electromagnetic field for the ground, n_1, and excited, n_2, states. Time-dependent current at the left interface, I_L, is shown in Fig. 3(b). Parameters of the calculation are $T=300$ K, $\varepsilon_1=-1$ eV, $\varepsilon_2=1$ eV, $[\mathbf{\Gamma}_K]_{mm}=0.1$ eV, and $[\mathbf{\Gamma}_K]_{12}=[\mathbf{\Gamma}_K]_{21}=0$ ($m=1,2$ and $K=L,R$). For interaction with electromagnetic field, we take $\vec{\mu}\vec{E}_0=0.005$ eV, where $\vec{E}_0$ is amplitude of the external laser field before enhancement. Bias V is applied symmetrically $\mu_{L,R}=E_F\pm eV/2$, and the Fermi energy is $E_F=0$. Results presented in Fig. 3 are obtained for bowtie geometry with 10 nm gap at bias $V=2$ V. Exact numerical calculation (solid line) is compared with adiabatic approximation data (dashed line). One sees that the adiabatic approximation for realistic parameters provides qualitatively correct results. It misses however delay (memory) effects and overestimates response signal. Electromagnetic pulse depletes ground state and populates excited state, which for the chosen bias leads to increase in current through the junction due to increase in transmission of the excited-state channel (see discussion of Fig. 5 below).

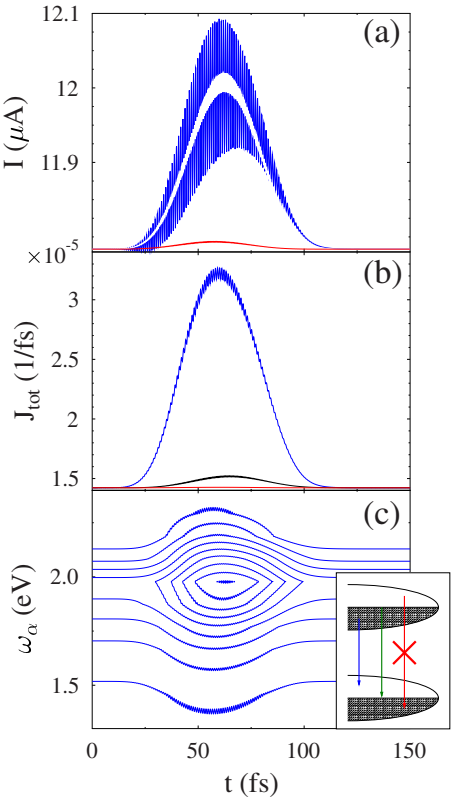

FIG. 4. (Color online) The two-level (HOMO-LUMO) model. Shown are (a) current and (b) total optical response, Eq. (24), vs time for bowtie inanimateness (the strongest signal, blue) and two spheres junction geometries. In the latter case, the response is calculated for two positions of the molecule in the junction: in the middle between the spheres (the weakest signal, red) and closer to one of the spheres [intermediate signal, (a) white silhouette and (b) solid line, black]. (c) shows contour map of optical flux, Eq. (23), for bowtie geometry vs outgoing frequency and time. A sketch of optical transitions at different frequencies is shown in the inset. See text for parameters.

We compare response of the two molecular junction geometries in Fig. 4. Bowtie geometry provides stronger local enhancement, and consequently stronger molecular response. In the case of spherical nanoparticles, we consider two possible positions of molecule between the electrodes: symmetric and asymmetric (3 nm shift from the center, where the field enhancement for the geometry is strongest). These yield weakest and intermediate signal, respectively. Note that it is natural to expect that local-field enhancement is stronger for a structure with uneven surface. Figure 4(a) presents time-dependent current for the three cases. Total optical response, Eq. (24), is shown in Fig. 4(b). We choose $\eta=5\times10^{-5}$ and $\omega_c=2$ eV, other parameters are as in Fig. 3. Note much more sensitive character of optical response to resonant conditions. Increase in fluorescence depends on population buildup in the excited state. The latter is much stronger for bowtie signal. At the same time, current does not necessarily requires physical population of the excited state (increase due to superexchange contribution). Figure 4(c) shows time-dependent optical spectrum, Eq. (23), for the bowtie geometry. The signal follows (with a delay) the pulse of the

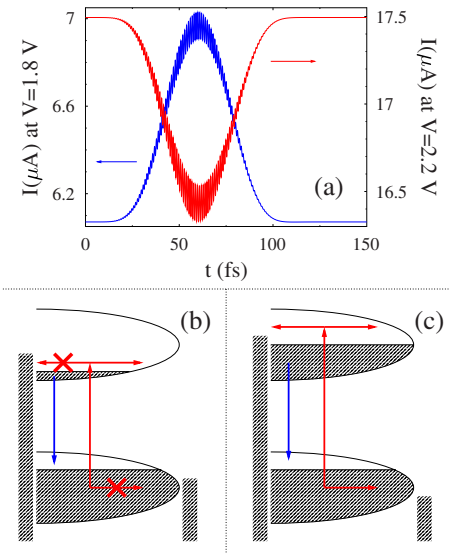

FIG. 5. (Color online) Shown are (a) current vs time for the two-level (HOMO-LUMO) model calculated at two different biases, and two sketches of optical pulse influence on current at (b) prearrangement, $V\sim 1.8$ V and (c) postrecession, $V\sim 2.2$ V bias. See text for parameters.

external field. Asymmetric character of the spectrum relative to resonance, $\omega_\alpha=2$ eV, is due to the fact that higher frequencies correspond to transitions between higher-energy parts of the excited-state Lorentzian and lower-energy parts of the ground-state Lorentzian. Since the former are predominantly empty and the latter are mostly filled, fluorescence due to this transition is diminished (see inset).

Figure 5(a) shows time-dependent current response to external driving at two different constant biases. The calculation is done for bowtie geometry with a gap of 10 nm, parameters are the same as in Fig. 3.

At pre-resonant bias, $V=1.8$ eV, before the field is applied, ground state is almost completely filled and excited state is almost empty. Thus optical excitation at resonance frequency is very effective in transferring electrons from ground into excited state. Since, current through the ground state is mostly blocked by the contact Fermi distributions, and channel through excited state is open, bringing charge carriers into excited Lorentzian leads to increase in the total current through the junction [see sketch in Fig. 5(b)]. This situation is similar to the effect of optical excitation on transport presented in Fig. 3(b). However, more favorable initial ground- and excited-states populations lead to a stronger increase in the current as a result of optical excitation.

At post-resonant bias, $V=2.2$ eV, populations in excited and ground states are similar. This is unfavorable for electron transfer between channels blocked in the ground state and open in the excited state. Instead, electrons are mostly transferred from open channels with high transition probability in the ground state into lower transition-probability channels in the excited state. Also part of the latter are coupled to empty continua on both sides of the junction. Thus depletion of the open ground-state channels leads to decrease in the total current in this case [see sketch in Fig. 5(c)]. Note, that at even higher biases, $V\sim 3$ eV optical pulse will not change total current.

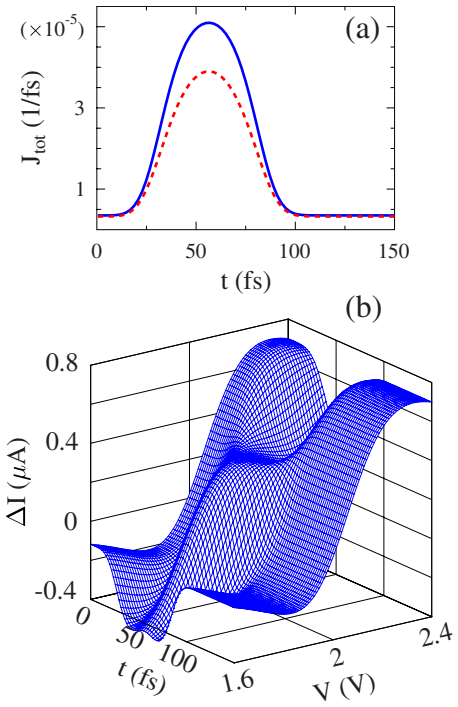

FIG. 6. (Color online) Role of energy-transfer process. Shown are (a) total optical response vs time with (dotted line, red) and without (solid line, blue) electron-hole excitations and (b) difference, $\Delta I=I_0-I_{e\text{-}h}$, between current calculated without (I_0) and with ($I_{e\text{-}h}$) electron-hole excitations vs time and bias. Calculations are performed within adiabatic approximation scheme. See text for parameters.

Calculations so far disregarded influence of energy transfer, Eq. (7). Here we illustrate influence of energy-transfer process on time-dependent response of the junction within adiabatic approximation. Figure 6(a) shows total optical response calculated with (dashed line) and without (solid line) energy transfer included. The calculation is done for bowtie geometry with 10 nm gap at pre-resonant constant bias $V=1.8$ V. Other parameters are as in Fig. 3. As expected, energy transfer diminishes optical response of the junction since both energy transfer from molecule to contacts and fluorescence compete for the same excess electronic population in the excited state. Same result will be at resonance, $V=2$ V, and at post-resonant bias, $V=2.2$ V.

Figure 6(b) shows a map of difference $\Delta I\equiv I_0-I_{e\text{-}h}$ between current calculated without I_0 and with $I_{e\text{-}h}$ energy transfer taken into account vs time and bias. Parameters of the calculation are the same as in Fig. 3. Energy transfer is calculated within wideband approximation discussed in Ref. 18 with coupling parameter 0.1 eV.

Energy-transfer process facilitates transition of electronic population from excited to ground state, to electron-hole excitations in the contacts. In the absence of optical pulse, at pre-resonant bias $V=1.8$ V, electron population from excited-state open channels at the tail of Lorentzian (lower transition probability) are transferred to ground-state open channels with higher transition probability [see sketch in Fig. 5(b)], which leads to increase in total current. Thus, $\Delta I\equiv I_0-I_{e\text{-}h}<0$ for times close to 0 and 150 fs [see Fig. 6(b)].

Situation at post-resonant bias $V=2.2$ V in the absence of optical pulse is opposite. Due to higher population in the excited state, electron transfer to ground state becomes mostly from more conducting to less conducting channels [see sketch in Fig. 5(c)], as a result current drops, $\Delta I>0$ [Fig. 6(b) at t near 0 and 150 fs].

Electron transfer from ground to excited state due to laser pulse is less effective in the presence of energy transfer (it competes with the radiations decay). Since this transfer is favorable for increase in the current at $V=1.8$ V and its decrease at $V=2.2$ V (see discussion of Fig. 5), corresponding change will be less pronounced for the case when electron-hole excitations in the leads are taken into account. This results in increase (decrease) in ΔI for times t from 50 to 100 fs at V below (above) the threshold value of 2 V [see Fig. 6(b)].

So far our simulations were limited by relatively long laser pulses. If duration of incident pulse is longer than characteristic lifetime of the corresponding plasmon-polariton resonance, the only effect one observes is enhancement of electric field amplitude. Alternatively, short resonant laser pulse induces time-dependent phase in the total electric field. Here we illustrate the effect of local field on transport beyond field enhancement.

Lifetime of the plasmon-polariton resonance can be estimated from its quality factor,

$$Q = \frac{\lambda_r}{\Delta\lambda}, \tag{42}$$

where λ_r is the resonant wavelength and $\Delta\lambda$ is full width of the resonance at half maximum. Q represents number of oscillations of the system before it decays. Thus characteristic time of the plasmon-polariton resonance,

$$\tau_p \sim \frac{Q\lambda_r}{c} \sim \frac{\lambda_r^2}{\Delta\lambda c}, \tag{43}$$

where c is the speed of light in vacuum. For bowtie-antenna geometry with 5 nm gap lifetime of resonance at 602 nm is 19 fs. Figure 7 compares time-dependent current resulting from the local field driven by a 30 fs laser pulse and incident laser beam propagating in absence of metal surfaces. Local enhancement for the latter is taken into account by scaling the incident field to be comparable to a hot-spot signal. One sees that in addition to enhancement, presence of metal leads to delayed and longer response of a junction.

Chirped pulses were recently proposed as an optical control method for enhancing charge transfer in unbiased molecular junctions with strong charge-transfer transition.[65] Our approach being multilevel time-dependent scheme capable of treating arbitrary fields provides capability to study the effect in realistic systems and for realistic junction geometries.

VII. CONCLUSION

We consider a two-level (HOMO-LUMO) model of molecular junction driven by external time-dependent laser field. Finite-difference time-domain technique is used to calculate field distribution for two junction geometries. Resulting local field at the molecule is considered to be the driving force. We assume that the junction is initially in a nonequilibrium steady state resulting from applied constant bias. At time t_0, driving force (laser pulse) starts to influence the system. Time-dependent transport (charge flux through the junction) and optical response (photon flux from the molecule into accepting modes) are calculated for a set of geometries and applied biases. We rewrite a nonequilibrium Green's-function technique for time-dependent calculation in a form convenient for treating many-level molecular systems. Results of the simulations within the approach are compared to approximate scheme for an adiabatic pumping regime.

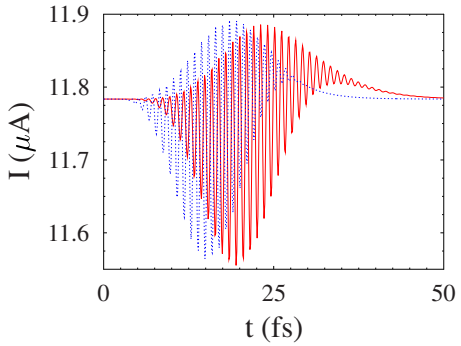

FIG. 7. (Color online) Effect of induced time-dependent phase on electron transport. Shown are time-dependent current resulting from incident monochromatic laser pulse (dotted line, blue) and local electric field with plasmon excitation induced time-dependent phase (solid line, red). The former is scaled to be comparable with enhanced local-field signal. Calculation is done for bowtie antennas with 5 nm gap. Incident pulse duration is 30 fs centered at $\lambda=602.6$ nm. Other parameters are as in Fig. 4

Our conclusions are: (1) nonequilibrium Green's-function approach is a useful tool for description of time-dependent transport beyond adiabatic approximation, short-time dynamics, and single-level model descriptions; (2) effect of locally enhanced fields on transport and optical response can be obtained theoretically, as is demonstrated by the model calculation with realistic parameters; (3) interplay of optical transitions and charge flux may lead to unexpected suppression of the current as a result of optical pulse.

Note that while our present consideration is restricted to driving force applied to the molecule only, generalization of the approach to situations of time-dependent bias and/or coupling between molecule and contacts is straightforward. Extension of the consideration to realistic molecular devices, taking into account time-dependent nonequilibrium distribution in the contacts and spatial profile of the field, and considering interplay of time dependencies of bias and laser field are goals of future research.

ACKNOWLEDGMENTS

The authors thank Abraham Nitzan for helpful discussions. M.S. is grateful to ASU financial and technical support (startup funds). M.G. gratefully acknowledges support by the UCSD (startup funds), the UC Academic Senate (research grant), and the U.S.-Israel Binational Science Foundation.

*maxim.sukharev@asu.edu
†migalperin@ucsd.edu

[1] S. A. Maier and H. A. Atwater, J. Appl. Phys. **98**, 011101 (2005).
[2] E. Ozbay, Science **311**, 189 (2006).
[3] W. A. Murray and W. L. Barnes, Adv. Mater. **19**, 3771 (2007).
[4] A. M. Schwartzberg and J. Z. Zhang, J. Phys. Chem. C **112**, 10323 (2008).
[5] E. Hutter and J. H. Fendler, Adv. Mater. **16**, 1685 (2004).
[6] A. J. Haes and R. P. Van Duyne, Expert Rev. Mol. Diagn. **4**, 527 (2004).
[7] R. Charbonneau, N. Lahoud, G. Mattiussi, and P. Berini, Opt. Express **13**, 977 (2005).
[8] A. K. Sarychev and V. M. Shalaev, *Electrodynamics of Metamaterials* (World Scientific, Singapore, 2007).
[9] H. Yokota, K. Saito, and T. Yanagida, Phys. Rev. Lett. **80**, 4606 (1998).
[10] H. Raether, *Surface Plasmons on Smooth and Rough Surfaces and on Gratings* (Springer, Berlin, 1988).
[11] U. Kreibig and M. Vollmer, *Optical Properties of Metal Clusters* (Springer, New York, 1995).
[12] K. Lopata and D. Neuhauser, J. Chem. Phys. **130**, 104707 (2009).
[13] K. Lopata and D. Neuhauser, J. Chem. Phys. **131**, 014701 (2009).
[14] M. G. Reuter, M. Sukharev, and T. Seideman, Phys. Rev. Lett. **101**, 208303 (2008).
[15] S. W. Wu, G. V. Nazin, and W. Ho, Phys. Rev. B **77**, 205430 (2008).
[16] D. R. Ward, N. J. Halas, J. W. Ciszek, J. M. Tour, Y. Wu, P. Nordlander, and D. Natelson, Nano Lett. **8**, 919 (2008).
[17] Z. Ioffe, T. Shamai, A. Ophir, G. Noy, I. Yutsis, K. Kfir, O. Cheshnovsky, and Y. Selzer, Nat. Nanotechnol. **3**, 727 (2008).
[18] M. Galperin and A. Nitzan, J. Chem. Phys. **124**, 234709 (2006).
[19] M. Galperin, M. A. Ratner, and A. Nitzan, J. Chem. Phys. **130**, 144109 (2009).
[20] E. G. Petrov, V. May, and P. Hänggi, Chem. Phys. **319**, 380 (2005).
[21] E. G. Petrov, V. May, and P. Hänggi, Phys. Rev. B **73**, 045408 (2006).
[22] M. Koentopp, C. Chang, K. Burke, and R. Car, J. Phys.: Condens. Matter **20**, 083203 (2008).
[23] G. Stefanucci and C.-O. Almbladh, Europhys. Lett. **67**, 14 (2004).
[24] S. Kurth, G. Stefanucci, C.-O. Almbladh, A. Rubio, and E. K. U. Gross, Phys. Rev. B **72**, 035308 (2005).
[25] J. N. Pedersen and A. Wacker, Phys. Rev. B **72**, 195330 (2005).
[26] I. V. Ovchinnikov and D. Neuhauser, J. Chem. Phys. **122**, 024707 (2005).
[27] M. Esposito and M. Galperin, Phys. Rev. B **79**, 205303 (2009).
[28] M. G. Schultz and F. von Oppen, Phys. Rev. B **80**, 033302 (2009).
[29] M. Leijnse and M. R. Wegewijs, Phys. Rev. B **78**, 235424 (2008).
[30] M. Galperin and S. Tretiak, J. Chem. Phys. **128**, 124705 (2008).
[31] A. P. Jauho, N. S. Wingreen, and Y. Meir, Phys. Rev. B **50**, 5528 (1994).
[32] M. P. Anantram and S. Datta, Phys. Rev. B **51**, 7632 (1995).
[33] B. Wang, J. Wang, and H. Guo, Phys. Rev. Lett. **82**, 398 (1999).
[34] A. Prociuk and B. D. Dunietz, Phys. Rev. B **78**, 165112 (2008).
[35] A. R. Hernández, F. A. Pinheiro, C. H. Lewenkopf, and E. R. Mucciolo, Phys. Rev. B **80**, 115311 (2009).
[36] M. Galperin and A. Nitzan, Phys. Rev. Lett. **95**, 206802 (2005).
[37] D. Kienle, M. Vaidyanathan, and F. Léonard, arXiv:1003.2058, Phys. Rev. B (to be published).
[38] P. Myöhänen, A. Stan, G. Stefanucci, and R. van Leeuwen, Phys. Rev. B **80**, 115107 (2009).
[39] M. Galperin, A. Nitzan, and M. A. Ratner, Phys. Rev. B **78**, 125320 (2008).
[40] M. Besbes, J. P. Hugonin, P. Lalanne, S. van Haver, O. T. A. Jansse, A. M. Nugrowati, M. Xu, S. F. Pereira, H. P. Urbach, J. Eur. Opt. Soc. Rapid Publ. **2**, 07022 (2007).
[41] A. Taflove and S. C. Hagness, *Computational Electrodynamics: The Finite-Difference Time-Domain Method*, 3rd ed. (Artech House, Boston, 2005).
[42] S. K. Gray and T. Kupka, Phys. Rev. B **68**, 045415 (2003).
[43] T. Kashiwa and I. Fukai, Microwave Opt. Technol. Lett. **3**, 203 (1990).
[44] J. P. Berenger, in *Perfectly Matched Layer (PML) for Computational Electromagnetics*, Synthesis Lectures on Computational Electromagnetics, edited by C. A. Balanis (Morgan and Claypool, San Rafael, CA, 2007).
[45] J. A. Roden and S. D. Gedney, Microwave Opt. Technol. Lett. **27**, 334 (2000).
[46] M. Sukharev, J. Sung, K. G. Spears, and T. Seideman, Phys. Rev. B **76**, 184302 (2007).
[47] M. I. Stockman, S. V. Faleev, and D. J. Bergman, Phys. Rev. Lett. **88**, 067402 (2002).
[48] T.-W. Lee and S. K. Gray, Phys. Rev. B **71**, 035423 (2005).
[49] G. D. Mahan, *Many-Particle Physics* (Kluwer Academic/Plenum, New York, 2000).
[50] S. Mukamel, *Principles of Nonlinear Optical Spectroscopy* (Oxford University Press, New York, 1995).
[51] H. Haug and A.-P. Jauho, *Quantum Kinetics in Transport and Optics of Semiconductors* (Springer, New York, 2008).
[52] A. Nitzan, *Chemical Dynamics in Condensed Phases* (Oxford University Press, New York, 2006).
[53] D. Lauvergnat, S. Blasco, X. Chapuisat, and A. Nauts, J. Chem. Phys. **126**, 204103 (2007).
[54] W. Magnus, Commun. Pure Appl. Math. **7**, 649 (1954).
[55] D. Prato and P. W. Lamberti, J. Chem. Phys. **106**, 4640 (1997).
[56] P. Zhang, Q.-K. Xue, and X. C. Xie, Phys. Rev. Lett. **91**, 196602 (2003).
[57] J. Fransson and J.-X. Zhu, Phys. Rev. B **78**, 113307 (2008).
[58] M. Galperin, A. Nitzan, and M. A. Ratner, Phys. Rev. Lett. **96**, 166803 (2006).
[59] W. H. Press, S. A. Teukolsky, W. T. Vetterling, and B. P. Flannery, *Numerical Recipes in C* (Cambridge University Press, Cambridge, England, 1994).
[60] M. Di Ventra, S. T. Pantelides, and N. D. Lang, Phys. Rev. Lett. **84**, 979 (2000).
[61] I. Kinoshita, A. Misu, and T. Munakata, J. Chem. Phys. **102**, 2970 (1995).
[62] M. Ponder and R. Mathies, J. Phys. Chem. **87**, 5090 (1983).
[63] V. L. Colvin and A. P. Alivisatos, J. Chem. Phys. **97**, 730 (1992).
[64] A. Kinkhabwala, Z. Yu, S. Fan, Yu. Avlasevich, K. Müllen, and W. E. Moerner, Nat. Photonics **3**, 654 (2009).
[65] B. D. Fainberg, M. Jouravlev, and A. Nitzan, Phys. Rev. B **76**, 245329 (2007).